Thermodynamics of Charge Separation of Photosystem I in the *menA* and *menB* Null Mutants of *Synechocystis* sp. PCC 6803 Determined by Pulsed Photoacoustics[†]

Harvey J. M. Hou,*[,‡] Gaozhong Shen,[§] Vladimir A. Boichenko,[||] John H. Golbeck,[§] and David Mauzerall*[,⊥]

Department of Chemistry and Biochemistry, University of Massachusetts Dartmouth, North Dartmouth, Massachusetts 02747, Department of Biochemistry and Molecular Biology and Department of Chemistry, The Pennsylvania State University, University Park, Pennsylvania 16802, Institute of Basic Biological Problems, Russian Academy of Sciences, Pushchino 142290, Russia, and The Rockefeller University, 1230 York Avenue, New York, New York 10065

Received October 18, 2008; Revised Manuscript Received January 11, 2009

ABSTRACT: When the biosynthesis of phylloquinone is inhibited in *Synechocystis* sp. PCC 6803 by interrupting the *menA* or the *menB* gene, photosystem I (PS I) recruits plastoquinone-9 (A_P) to occupy the A_1 sites. In PS I from the *menA* and *menB* null mutants, forward electron transfer from the quinone to the FeS clusters occurs approximately 1000 times slower than in wild-type PS I [Semenov, A. Yu., Vassiliev, I. R., van der Est, A., Mamedov, M. D., Zybailov, B., Shen, G., Stehlik, D., Diner, B. A., Chitnis, P. R., and Golbeck, J. H. (2000) *J. Biol. Chem. 275*, 23429−23438]. To investigate the effect on thermodynamics, the enthalpy and volume changes of charge separation in PS I in the *menA* and *menB* mutants were measured using pulsed time-resolved photoacoustics on the nanosecond and microsecond time scales. The observed thermodynamic data are the same for the *menA* and *menB* mutants. This is expected because the recruited quinone (A_P) is the same in both mutants. The volume change of PS I from the mutants following charge separation on both time scales was -17 ± 2 Å^3, less than that of the wild type, -21 Å^3. The quantum yield of charge separation was found to be slightly lower ($85 \pm 9\%$) than that of wild-type PS I ($96 \pm 10\%$). The observed reaction is assigned to the formation of $P_{700}{}^+A_P{}^-$ from $P_{700}{}^*A_P$. An enthalpy change (ΔH) of -0.69 ± 0.07 eV was obtained for this reaction. In contrast, a larger enthalpy change -0.8 eV for the formation of $P_{700}{}^+A_1{}^-$ from $P_{700}{}^*$ and an apparent entropy change ($T\Delta S$, $T = 25$ °C) of -0.2 eV were obtained in wild-type PS I [Hou, H. J. M., and Mauzerall, D. (2006) *J. Am. Chem. Soc. 128*, 1580−1586]. Taking the free energy to be -0.70 eV in PS I of the mutants, the apparent entropy is close to zero in the mutants. Since the apparent entropy change for the overall reaction of the production of $P_{700}{}^+F_{A/B}{}^-$ from $P_{700}{}^*$ is very likely the same as that of the wild type, $+0.35$ eV, this implies that the reaction of $P_{700}{}^+A_P{}^-F_{A/B} \rightarrow P_{700}{}^+A_PF_{A/B}{}^-$ in the mutants is almost completely entropy driven ($\Delta G = -0.07$ eV and $T\Delta S = +0.40$ eV). These results show that not only the kinetics but also the thermodynamics of electron transfer reactions in PS I are significantly affected by the recruitment of the foreign plastoquinone-9 into the A_1 site.

Two types of photosynthetic reaction centers exist in nature. Type I reaction centers incorporate a phylloquinone or menaquinone as secondary acceptor, A_1,[1] and three tertiary iron−sulfur cluster acceptors, F_X, F_B, and F_A. Type II reaction centers incorporate two quinone acceptors; Q_A undergoes a one-electron reduction, and Q_B undergoes a two-electron reduction with concomitant protonation. Oxygenic photosynthesis in cyanobacteria, algae, and higher plants involves the serial cooperation of photosystem I (PS I), a type I reaction center, and photosystem II (PS II), a type II reaction center (*1*). Both types of photosynthetic reaction centers contain a quinone that operates as an intermediate electron acceptor and as a one-electron carrier. However, the local protein environment and chemical properties of the quinone in these two types of reaction centers must be different. For example, EPR measurements revealed that there are striking differences in the binding and function of phylloquinone (A_1) in PS I and ubiquinone (Q_A) in the bacterial center of *Rhodobacter sphaeroides*, a type II reaction center (*2, 3*).

[†] The work was supported by previous and current grants from the National Science Foundation (MCB-9904522 to D.M. and MCB-0519743 to J.H.G.) and by the UMass Dartmouth Chancellor's Research Fund (to H.J.M.H.).

* To whom correspondence should be addressed. D.M.: tel, (212) 327-8218; fax, (212) 327-8853; e-mail, mauzera@mail.rockefeller.edu. H.J.M.H.: tel, (508) 999-8234; fax, (508) 999-9167; e-mail, hhou@umassd.edu.

[‡] University of Massachusetts Dartmouth.

[§] The Pennsylvania State University.

[||] Russian Academy of Sciences.

[⊥] The Rockefeller University.

[1] Abbreviations: A_1, phylloquinone molecule a secondary electron acceptor in wild-type PS I; A_P, plastoquinone-9 molecule recruited into the A_1 site in PS I mutants replacing the phylloquinone; Asc, sodium ascorbate, DM, *n*-dodecyl β-D-maltopyranoside; HEPES, *N*-(2-hydroxyethyl)piperazine-*N*′-2-ethanesulfonic acid; *menA*, gene that codes for the 1,4-dihydroxy-2-naphthoate octaprenyl transferase in *Synechocystis* sp. PCC 6803; *menB*, gene that codes for the 1,4-dihydroxy-2-naphthoic acid synthase in *Synechocystis* sp. PCC 6803; MOPS, 3-(*N*-morpholino)propanesulfonic acid; PA, photoacoustic(s); PMS, phenazine methosulfate; PS I, photosystem I; TE, thermal efficiency; Φ, quantum yield of photochemistry in PS I; σ, optical cross section; α', apparent expansivity, which is the thermal expansivity divided by the heat capacity and density; κ, compressibility; ε, dielectric constant.

10.1021/bi801951t CCC: $40.75
Published on Web 02/05/2009

Cyanobacterial PS I, a pigment−protein complex consisting of at least 11 polypeptides embedded in the photosynthetic membrane, catalyzes light-induced electron transfer from reduced plastocyanin (or cytochrome c_6) to oxidized ferredoxin (or flavodoxin) (*4, 5*). The kinetics of electron transfer in PS I has been established (*6, 7*). The energy of a photon is absorbed by the light-harvesting chlorophylls. The absorbed light energy is efficiently transferred to the primary donor P_{700} (a pair chlorophyll *a* molecules) in several hundred femtoseconds. The excited P_{700}* passes an electron to the primary acceptor A_0 (a chlorophyll *a* monomer) in 3−14 ps. The reduced A_0^- donates its electron to the secondary acceptor A_1 (a phylloquinone) in 50 ps. The reduced A_1^- delivers its electron to F_X (an iron−sulfur cluster) in 20 and 200 ns. Finally, the reduced F_X^- gives its electron to F_A and F_B in 50−200 ns.

The recent three-dimensional structure of cyanobacterial PS I at 2.5 Å resolution (*8*) and plant PS I at 3.4 Å resolution (*9*) has revealed much of the detailed orientation and binding site of phylloquinone, thereby providing a solid basis for structure and function studies at an atomic level. The kinetic data of site-directed mutants from *Chlamydomonas reinhardtii* suggest that both of the phylloquinones in PS I are involved in active electron transfer albeit with different kinetic constants (*10−12*). This observation is intriguing because it indicates that both branches of electron transfer factors are nearly equally active (about 60−65% A-side electron transfer) in PS I of green alga. In contrast, experimental data reported in cyanobacteria imply an asymmetric electron transfer with approximate 75−80% A-side electron transfer contribution (*13−16*).

It has been generally accepted that unlike ubiquinone (Q_A) in bacterial centers from *Rb. sphaeroides*, which can be easily replaced by a wide variety of different quinines, phylloquinone is difficult to dislodge from the A_1 binding sites in PS I (*17, 18*). A biological method to replace phylloquinone was recently devised. Targeted inactivation of the *menA* and *menB* genes that code for phytyl transferase and naphthoate synthase in the phylloquinone biosynthetic pathway (*19*) precludes its availability for incorporation in the A_1 site. Yet, in spite of the demonstrated absence of phylloquinone, the *menA* and *menB* null mutants grow photosynthetically. EPR measurements show that plastoquinone-9 (A_P) has been recruited into the A_1 site and functions as an efficient one-electron electron carrier (*20*). Time-resolved optical studies indicate the forward electron transfer from A_1^- to F_X is slowed 1000-fold, to 15 and 300 μs, compared to 20 and 200 ns in the wild type (*21*). Given the altered kinetics of electron transfer, it was of interest to investigate the effect of these molecular replacements on the thermodynamics of electron transfer in PS I.

Pulsed time-resolved photoacoustics can provide a direct measurement of thermodynamic parameters such as volume changes (ΔV) and enthalpy changes (ΔH) that accompany electron transfer reactions (*22−41*). With prior knowledge of the change in Gibbs free energy of the corresponding reactions, the entropy change ($T\Delta S$) of the reaction can be calculated. This is an important parameter, knowledge of which is required to fully understand the mechanism of electron transfer, and it has been largely underreported in the literature. The ΔH, ΔV, and $T\Delta S$ of electron transfer in the photosynthetic reaction center from *Rb. sphaeroides* (*18, 39*) have been measured using pulsed photoacoustics. In oxygenic photosynthetic systems, the same parameters of electron transfer in PS I trimers and in Mn-depleted PS II reaction center cores from *Synechocystis* sp. PCC 6803 and higher plants have been investigated using similar techniques (*33, 42*). These data were confirmed by photoacoustic measurements on whole cells of *Synechocystis* sp. PCC 6803 (*34*). The thermodynamic parameters of bacterial reaction centers were found to be similar to those of PS I and dramatically different from those of PS II.

Using the fit by convolution of photoacoustic waves on the nanosecond and microsecond time scales, we were able to resolve the thermodynamic parameters of different kinetic steps in *Synechocystis* PS I (*35*). We obtained a large negative enthalpy (−0.8 eV) and large volume change (−23 Å^3) for the $P_{700}^* \rightarrow A_1^-F_X$ step and a positive enthalpy (+0.4 eV) and a small volume change (−3 Å^3) for the $A_1^-F_X \rightarrow F_{A/B}^-$ step. For the fast reaction the free energy change for the $P_{700}^* \rightarrow A_1^-F_X$ step is −0.63 eV, and the entropy change ($T\Delta S$, $T = 25$ °C) is −0.2 eV. For the slow reaction, $A_1^-F_X \rightarrow F_{A/B}^-$, the free energy is −0.14 eV (*43*), and the entropy change ($T\Delta S$) is positive, +0.54 eV. The positive entropy contribution is even larger than the positive enthalpy, indicating that the A^-F_X to $F_{A/B}^-$ step in *Synechocystis* PS I is entropy driven.

The objective of the present work is to extract the thermodynamic parameters of electron transfer in the *menA* and *menB* null mutants of PS I (hereafter known as *menA*/*B* PS I) on both the nanosecond and microsecond time scales. In these two mutants, phylloquinone in the A_1 site of PS I has replaced by plastoquinone-9. We carried out the present studies to explore possible differences caused by molecular replacement of phylloquinone with plastoquinone-9 on the thermodynamics of the peculiar A^- to F_{AB}^- step.

EXPERIMENTAL PROCEDURES

Preparation of Purified PS I Trimers. PS I trimers from the *menA* and *menB* null mutants and the wild-type strains of *Synechocystis* sp. PCC 6803 were isolated and purified according to published methods (*19, 44, 52, 53*).

Photoacoustic Measurements. The microsecond time-resolved photoacoustic setups are designed for the PA measurements on an ~1 μs time scale at a time resolution of ~100 ns (*18*), and the procedures for measurement were described previously (*32*) as were the nanosecond time-resolved photoacoustic measurements with a time resolution of ~10 ns (*35*).

RESULTS

Volume Contraction on the Microsecond Time Scale. The photoacoustic signal is detected as a pressure wave in the medium caused by a time-dependent volume change, both thermal and intrinsic, upon excitation with light. Figure 1 shows the typical photoacoustic signals of the purified PS I trimers prepared from the *menA*/*B* null mutants and the wild-type strains of *Synechocystis* sp. PCC 6803 on the microsecond time scale. The PA reference ink (Figure 1, curve 1) showed a large, positive amplitude upon illumination at 25 °C, which is the fast heat release of all of the light energy absorbed by the ink. Its amplitude is the measure of the

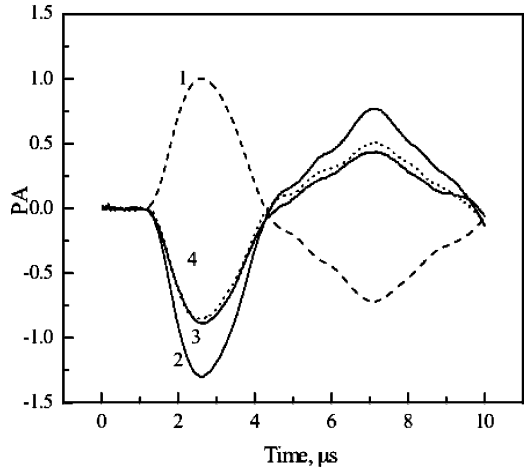

FIGURE 1: PA signals of *menA* PS I, *menB* PS I, and wild-type PS I on the microsecond time scale. (1) PA reference ink, the OD value at 680 nm was ~2.0/cm, pH 8.0, 10 mM HEPES, 0.03% DM, 25 °C, flash energy at ~2 μJ cm^{-2}. (2) WT PS I, 60 μM PMS, 2 mM Asc, 3.8 °C. (3) *menA* PS I, 60 μM PMS, 2 mM Asc, 3.8 °C. (4) *menB* PS I, 60 μM PMS, 2 mM ASC, 3.8 °C.

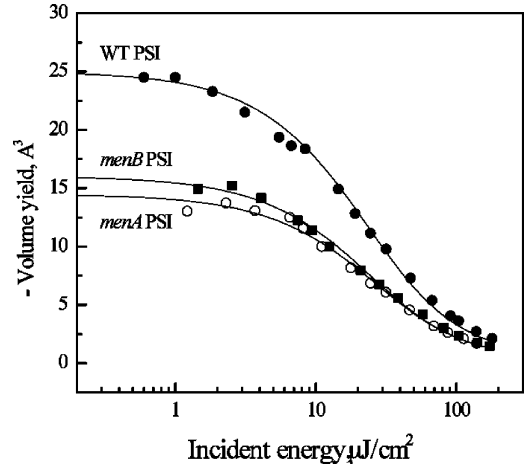

FIGURE 2: Volume yield curves of *menA* PS I, *menB* PS I, and wild-type PS I on the microsecond time scale. pH 8.0, 10 mM HEPES, the OD value of PS I samples at 680 nm was ~2.0/cm, 60 μM PMS, 2 mM Asc, 0.03% DM, excitation at 680 nm, 3.8 °C. The vertical axis is volume per absorbed photon per center. The lines are the fit of experimental data using the equation $\Delta V_{sc}/E = N\Delta V_y(1 - e^{-\Phi\sigma E})/N\sigma E$. (1) WT PS I, $\phi\Delta V_y = 24.6 \pm 2$ Å^3, $\sigma = 200 \pm 20$ Å^2. (2) *menA* PS I, $\phi\Delta V_y = 14 \pm 2$ Å^3, $\sigma = 176 \pm 18$ Å^2. (3) *menB* PS I, $\phi\Delta V_y = 16 \pm 2$ Å^3, $\sigma = 165 \pm 18$ Å^2. For detailed theory, see ref (*32*).

photon energy absorbed by the sample (E_a), the piezo film sensitivity (F), the apparent expansivity ($\alpha' =$ thermal expansivity/heat capacity $\times$ density), and the compressibility (κ) (*32*).

The PA signals produced by forming a charge-separated radical pair upon light excitation of PS I trimers consist of at least two major components: (1) the heat output (Q_{RC}), which includes the enthalpy change of the reaction and other rapidly released heat, and (2) the volume change of the reaction (ΔV_{RC}). The thermal signal disappears at the temperature of maximum density of the suspending medium, T_m, near or below 4 °C, because at that temperature, $\alpha' = 0$, thus leaving only the volume term. Wild-type PS I trimers produced large negative PA signals at 3.8 °C (Figure 1, curve 2) which originate directly from the volume contraction via electrostriction (*22*). The wild-type PS I signal has a relative amplitude of −1.3, corresponding to −25 Å^3, when normalized to peak-to-peak amplitude of the PA reference signal. In contrast, *menA*/*B* PS I shows a smaller signal with a relative amplitude of −0.9 (Figure 1, curves 3 and 4). There is no major difference in the volume contraction between *menA* PS I and *menB* PS I. This may be expected since plastoquinone-9 is present in the A_1 sites in PS I in both mutants (*19*).

To confirm the values of the volume change and to estimate the quantum yield of charge separation in *menA*/*B* PS I, we used two different approaches: (1) volume yield measurements and (2) saturation measurements. The detailed description of these two procedures has been given previously (*32*).

The fits of the volume yield curves for the mutants and wild-type PS I are shown in Figure 2. The apparent volume contractions of *menA* PS I and *menB* PS I are −14 and −16 Å^3, respectively, compared to −25 Å^3 for wild-type PS I (Table 1). It is worthy of note that, in this first method, at low energy one obtains the apparent volume change, which is the volume per center (ΔV_y) multiplied by the quantum yield (Φ). An easy explanation of the smaller values in the mutant PS I samples may be a low quantum yield, for example, $\Phi = \sim 0.5$. However, as shown below, our experimental data in the second method show that this is probably not the case.

In the second saturation method, we aim to excite every PS I complex to obtain the maximum PA signal. In this method, one must calculate the number of PS I centers in the illuminated volume of the cell (~0.34 mL), N, to obtain the real volume change ΔV_s. We stress that, in this analytical method, the volume change does not contain the quantum yield. As shown in Figure 3, the saturation value of volume change (ΔV_s) in *menA*/*B* PS I was ~−17 Å^3, which is slightly higher than that using the volume yield method. These findings confirm the previous results and argue that the quantum yield of photochemistry in the mutants is not low. We will now discuss this issue in more detail.

The quantum yield of photochemistry can be estimated from measurements of the effective cross section ($\Phi\sigma$), which is directly obtained from the fit of the saturation curves (Table 1). Taking the calculated cross section of 195 Å^2 for PS I (*32*), the quantum yield of charge separation in *menA*/*B* PS I was estimated to be 85% (Table 1), a value slightly lower than the 96% quantum yield in wild-type PS I.

This view is supported by the fact that the volume changes obtained by the two methods are very similar. In *menA* PS I and *menB* PS I, the volume change ($\Phi\Delta V_y$) is −14 to −16 Å^3, respectively, which is ~15% (i.e., $\Phi = 0.85$) smaller than the saturation value (ΔV_s) of −16 to 18 Å^3. The latter is the absolute number, calculated without assumptions, of the quantum yield assuming all centers are successfully "hit". Note that these two plots (Figures 2 and 3) are of the same data, differently weighted. However, the calculation of ΔV is completely different. The first, being linear, is a simple ratio to the reference. The second requires knowledge of the number of centers in the light-saturated volume. Taken together, they suggest that the volume contractions in *menA*/*B* PS I on the microsecond time scale are −17 ± 2 Å^3, and the quantum yields of photochemistry are ca. 85 ± 10%. The observed reaction on the microsecond time scale is

Table 1: Volume Contraction, Effective Optical Cross Section, Quantum Yield, Thermal Efficiency, and Enthalpy of Charge Separation on the Microsecond Time Scale in *menA* and *menB* PS I and Wild-Type PS I Trimers Isolated from *Synechocystis* sp. PCC 6803

sample[a]	$\Phi\Delta V_y$[b] (Å^3)	ΔV_s[c] (Å^3)	σ (Å^2)	Φ[d] (%)	TE_0 (%)	ΔH[e] (eV)
menA PS I	-15 ± 2	-17 ± 2	165 ± 18	83 ± 9	53 ± 5	-0.64 ± 0.06
menB PS I	-16 ± 2	-18 ± 2	170 ± 17	87 ± 9	51 ± 5	-0.74 ± 0.07
WT PS I	-25 ± 2	-26 ± 2	190 ± 19	96 ± 10	76 ± 3	-0.40 ± 0.04

[a] pH 8.0, 10 mM HEPES, 0.03% DM, 60 μM PMS, and 2 mM Asc. [b] The limiting value of the low energy yield curve fit at 3.8 °C. [c] The maximum value of saturating PA signal at 3.8 °C when all reaction centers are excited. [d] The values are obtained from the ratio of calculated optical cross sections of PS I, 195 Å^2 at 680 nm, to the effective optical cross sections $\Phi\sigma$. [e] The enthalpy changes are corrected by the measured quantum yield (*35*).

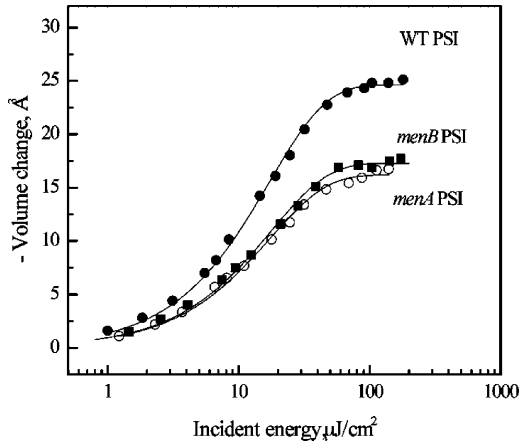

FIGURE 3: Saturation curve of *menA* PS I, *menB* PS I, and wild-type PS I on the microsecond time scale. Experimental conditions are the same as in Figure 2. The vertical axis is in units of volume per center. The lines are the fit of experimental data using the equation $\Delta V = N\Delta V_s(1 - e^{-\Phi\sigma E})$. (1) WT PS I, $\Delta V_s = 26 \pm 2$ Å^3, $\sigma = 190 \pm 19$ Å^2. (2) *menA* PS I, $\Delta V_s = 17 \pm 2$ Å^3, $\sigma = 165 \pm 18$ Å^2. (3) *menB* PS I, $\Delta V_s = 18 \pm 2$ Å^3, $\sigma = 170 \pm 18$ Å^2. For detailed theory, see ref *32*.

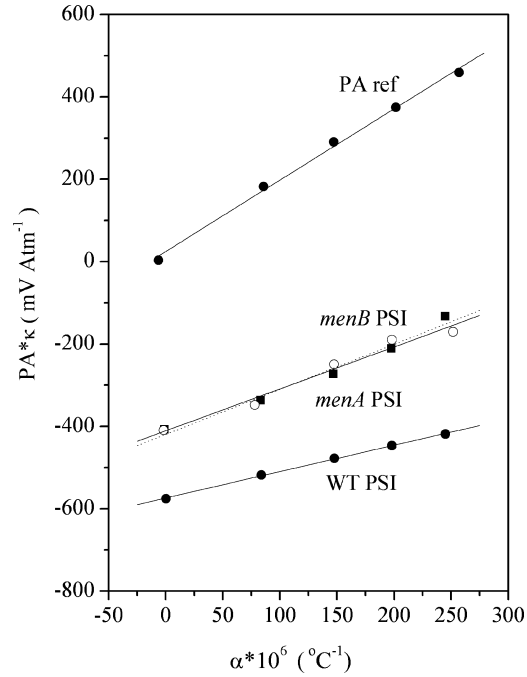

FIGURE 4: Analysis of the μs photoacoustic data of *menA* PS I, *menB* PS I, and wild-type PS I on the microsecond time scale. pH 8.0, 10 mM HEPES, the OD value of PS I samples at 680 nm was ~2.0/cm, 60 μM PMS, 2 mM ASC, 0.03% DM, flash energy is ~2 μJ/cm^2, excitation at 680 nm, 3.8 °C. Lines are the linear fit of the PA data of PA reference and the wild-type and mutant PS Is. The volume contraction and thermal efficiency of the *menA* PS I, *menB* PS I, and wild-type PS I were calculated by the intercept of the fits and difference in slopes: (1) *menA* PS I, $\Delta V = 15 \pm 2$ Å^3, TE = 53 ± 6%; (2) *menB* PS I, $\Delta V = 16 \pm 2$ Å^3, TE = 51 ± 5%; (3) WT PS I, $\Delta V = 25 \pm 2$ Å^3, TE = 76 ± 8%. For detailed calculation, see ref *32*.

attributed to the formation of $P_{700}{}^+F_{A/B}{}^-$ from excited $P_{700}{}^*$ for the wild-type PS I and of $P_{700}{}^+A_P{}^-$ for *menA*/*B* PS I.

Thermal Efficiency and Enthalpy Change on the Microsecond Time Scale. As stated above, PA signals produced by PS I trimers are composed of two components: a volume change (ΔV) and the release of heat (Q_{RC}). When we vary the temperature from 4 to 25 °C, the heat release should increase. In fact, the PA signals produced by *menA*/*B* PS I and wild-type PS I show a good linear dependence on α' when corrected for the effects of temperature on the compressibility factor (Figure 4). The intercept at $\alpha' = 0$ is the volume change. The ratio of slopes between the PS I trimers and PA reference ink gives the heat released during the electron transfer reaction in PS I (*32*). The values of thermal efficiency (TE) and enthalpy changes in the mutants and the wild-type PS I are listed in Table 1. The TE is the ratio of stored energy to that of the trap.

The thermal efficiency at 680 nm in *menA*/*B* PS I is ~52%, which is lower than the wild-type value of 76% (Table 1). Taking the quantum yield of 85% and a trap energy of 1.77 eV, the enthalpy changes (ΔH) of electron transfer in *menA* and *menB* PS I were calculated to be -0.64 ± 0.1 and -0.74 ± 0.07 eV, respectively. Since it is the complement of TE, the ΔH of electron transfer on the microsecond time scale in *menA*/*B* PS I is larger (-0.69 eV) than that in wild-type PS I (-0.40 eV).

Volume Contraction and Thermal Efficiency on the Nanosecond Time Scale. Figure 5 is the typical photoacoustic wave produced by a 0.1 mm photoacoustic cell, which enables one to focus on the fast nanosecond time scale reaction (for details see ref *35*). Curve 1 is the positive signal from a photoacoustic reference at 25 °C, and curves 2, 3, and 4 show large negative signals from wild-type PS I, *menA* PS I, and *menB* PS I, respectively, at 3.8 °C. They indicate that the volume contractions of the mutants are roughly two-thirds of the wild type and are similar to those on the microsecond time scale.

Figure 6 shows the analysis of photoacoustic data of the mutants and the wild type on the nanosecond time scale. We find that the volume changes during charge separation in *menA*/*B* PS I were smaller, -17 Å^3, than that of wild-type PS I, -21 Å^3 (Table 2). These values are identical to those of the mutants on the microsecond time scale, which indicate that there are no kinetic volume components between the 20 ns and 1 μs time scales in the mutants, in line with the kinetic data published previously (*21*). It also demonstrates that the photoacoustic methodology on both time scales is reliable and supports, indirectly, our conclusion of

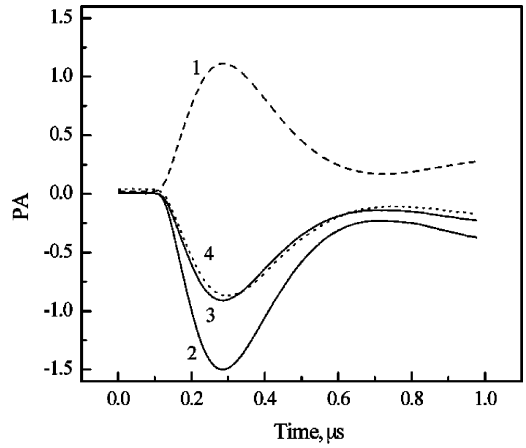

FIGURE 5: PA signals of *menA* PS I, *menB* PS I, and wild-type PS I on the nanosecond time scale. (1) PA reference ink, the OD value at 680 nm was ~20/cm, pH 8.0, 10 mM HEPES, 0.03% DM, 25 °C, flash energy at ~4 μJ cm^{-2}. (2) WT PS I, same OD value at 680 nm, 300 μM PMS, 2 mM Asc, at 3.8 °C. (3) *menA* PS I at 3.8 °C. (4) *menB* PS I at 3.8 °C.

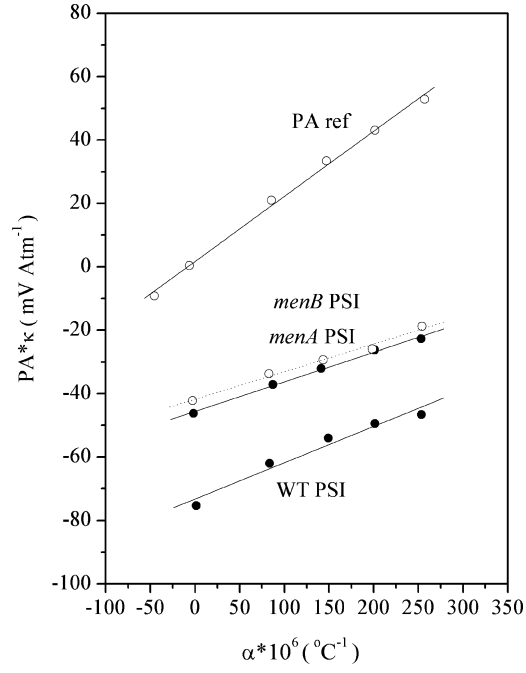

FIGURE 6: Analysis of the nanosecond photoacoustic data of *menA* PS I, *menB* PS I, and wild-type PS I. The conditions are the same as in Figure 5. Calculation followed the same procedures as in Figure 4. The results were as follows: (1) *menA* PS I, $\Delta V = 15 \pm 2$ Å^3, TE = 48 ± 6%; (2) *menB* PS I, $\Delta V = 14 \pm 2$ Å^3, TE = 55 ± 5%; (3) WT PS I, $\Delta V = 25 \pm 2$ Å^3, TE = 44 ± 5%.

a large enthalpy change in wild-type PS I on the nanosecond time scale (*35*).

The data in Figure 6 indicate that the thermal efficiency on the nanosecond time scale is 48−55% (Table 2), which is very close to that on the microsecond time scale. Thus we believe that no submicrosecond kinetic components are present in the mutants as judged by our photoacoustic results and by previous kinetic data.

Convolution Analysis of PA Signals. Our PA pressure wave signals are produced by volume changes of PS I trimers during the photochemical reaction. The convolution of the time derivative of the volume or heat release function with the apparatus response function provided by the reference signal enables us to resolve the fast and slow PA components (*25, 31, 35, 40, 45*). Optical kinetic studies on wild-type PS I show the time constant of electron transfer from P_{700}* to $F_{A/B}$ to be less than 200 ns (*46*−*50*). Convolution of the PA signal of the wild type with that of the reference resolved a <200 ns component with amplitude of −3 Å^3 and a prompt amplitude of −21 Å^3 at 3.8 °C (*35*). Using this convolution analysis we also resolved the positive enthalpy changes associated with the electron transfer step from A_1^- to $F_{A/B}$ in PS I (*35*).

Table 2: Volume Contraction, Thermal Efficiency, and Enthalpy of Charge Separation on the Nanosecond Time Scale in *menA* and *menB* PS I and Wild-Type PS I Trimers Isolated from *Synechocystis* sp. PCC 6803

sample[a]	$\Phi\Delta V$ (Å^3)	TE_0[b] (%)	ΔH[b] (eV)
menA PS I	−15 ± 2	48 ± 5	−0.75 ± 0.08
menB PS I	−14 ± 2	55 ± 5	−0.65 ± 0.07
WT PS I	−25 ± 2	44 ± 3	−0.99 ± 0.1

[a] pH 8.0, 10 mM HEPES, 0.03% DM, 60 μM PMS, and 2 mM Asc. [b] Thermal efficiency and enthalpy change were calculated with the trap energy of 1.77 eV (*35*).

For *menA*/*B* PS I, optical kinetic studies showed that electron transfer from A_P^- to F_X is much slower, with time constants of 15 and 300 μs (*21*). Our convolution analysis on the mutant data indicates there is at least one component with a lifetime longer than 10 μs at 3.8 °C with an uncertain, but substantial, amplitude (data not shown). The photoacoustic signal is a pressure wave caused by the rate of heat or volume production; thus the amplitude of the PA measurement is weighted by the rate constant of the heat-producing step. It is difficult to resolve steps longer than 10 μs because of the decrease in the signal amplitude and mixture with reflections in the cell. The analyses at higher temperatures to obtain ΔH were inconclusive because of the small time-resolved microsecond signals: the negative volume and positive enthalpy changes cancel.

To resolve the possible fast (nanosecond) components in the mutants, we conducted the photoacoustic measurements using our fast photoacoustic apparatus with a time resolution of ~10 ns. The results showed that the volume change (−15 Å^3) and thermal efficiency (~50%) in *menB* PS I are well in line with those (−17 Å^3 and ~51%) on the microsecond time scale (data not shown). This suggests that there is no fast component in the ~10 ns to 1 μs time range, which agrees with the kinetic data on the same mutant (*21*).

DISCUSSION

The *menA* gene codes for the 1,4-dihydroxy-2-naphthoate octaprenyl transferase enzyme in the phylloquinone biosynthetic pathway (*19*). The interruption of the *menA* gene in the cyanobacterium *Synechocystis* sp. PCC 6803 would be expected to block the attachment of the phytyl tail to the 2-carboxy-1,4-naphthoquinone substrate. The *menB* gene codes the 1,4-dihydroxy-2-naphthoic acid synthase enzyme in the phylloquinone biosynthetic pathway. The inactivation of the *menB* gene would be expected to block the cyclization of the ring to produce a 2-carboxy-1,4-naphthoquinone from the *O*-succinyl benzoyl-CoA substrate. The *menA* and *menB* null mutants of *Synechocystis* sp. PCC 6803 thus preclude the biosynthesis of phylloquinone and would be expected to show a similar phenotype (*19*). Both indeed lack phylloquinone, and both contain plastoquinone-9 in the A_1 sites of PS I.

There are two equally important factors for understanding mechanisms of electron transfer: kinetics and thermodynamics. Kinetics describes the details of electron transfer rates and intermediate states of electron pathways. Thermodynamics emphasizes the energy levels and driving forces of electron transfer in their initial and final states. The kinetic results, obtained by use of time-resolved optical and EPR techniques, showed that plastoquinone-9 functions as an efficient electron transfer cofactor in PS I, but with altered forward electron transfer kinetics (*21*). In terms of thermodynamics, only the redox potential of plastoquinone-9 in the A_1 site of PS I had been estimated (−0.61 V). Until the present work, there had been no information on volume, enthalpy, and entropy changes in PS I that contains plastoquinone-9. Here, we applied a pulsed photoacoustic technique to measure directly the volume change and heat release in electron transfer between excited P_{700} and the foreign quinone acceptor.

Volume Contraction. The volume contraction upon charge separation in photosynthesis is most likely produced by electrostriction. This parameter is directly related to charge separation and is an ideal measure of photochemical activity. The volume change in wild-type PS I is ca. −26 Å^3 (Tables 1 and 2), which is the same as the value reported previously (*32*). It is associated with electron transfer on formation of $P_{700}{}^+F_{A/B}{}^-$ from $P_{700}{}^*F_{A/B}$. In the case of *menA*/*B* PS I, PA measurements on the microsecond time scale reveal the volume contraction to be −17 Å^3 (Table 1). Considering our time window of 0.1−10 μs, this value is assigned to the formation of $P_{700}{}^+A_P{}^-$ from $P_{700}{}^*A_P$. We infer that the intermediate step of electron transfer from $P_{700}{}^+A_P{}^-F_{A/B}$ to $P_{700}{}^+A_PF_{A/B}{}^-$ would be accompanied by a volume change of −9 Å^3, assuming the replacement of A_1 with A_P causes no change in the $F_{A/B}$ clusters. This agrees with our convolution analysis of a slow negative component (amplitude uncertain).

For *menA*/*B* PS I, the size of the benzoquinone ring in plastoquinone-9 (A_P) is smaller than the naphthoquinone ring in phylloquinone. Electron spin−echo modulation experiments showed that the distance between $P_{700}{}^+$ and $A_P{}^-$ (25.3 Å) in *menA*/*B* PS I is the same as the distance between $P_{700}{}^+$ and $A_1{}^-$ in wild-type PS I (*20*). The volume contraction of electron transfer from P_{700} to A_P is estimated to be larger (−30 Å^3) than the observed one (−17 Å^3). Thus a positive volume due to a protein conformational change may be possible. The volume changes (+30 to +70 Å^3) due to protein conformational changes were observed in the photoreaction of bacteriorhodopsin and rhodopsin (*25, 40, 60*).

We offer a molecular explanation of the difference in the volume change predicted via electrostriction and that of the observed value (−17 Å^3). A simple explanation would be that the quantum yield of photochemistry is lower (for example, ∼0.7) in *menA*/*B* PS I. This, however, is unlikely because our pulse saturation data revealed a quantum yield of ∼85% in PS I from both mutants (Table 1), which is only sufficiently lower than the quantum yield of 96% in wild-type PS I to explain less than half of the effect. Further support for a high quantum yield is that the light saturation dependence of the flavodoxin reduction rate in *menA*/*B* PS I is similar to that of wild-type PS I (*19*). These two arguments are consistent in showing that the smaller volume change in the *menA*/*B* PS I is not caused by a low quantum yield.

Table 3: Volume Change, Enthalpy, and Apparent Entropy of Electron Transfer Reaction in PS I from the Wild Type and *menA*/*B* Null Mutants of *Synechocystis* sp. PCC 6803

	WT[a]	*menA*/*B*[b]
ΔV (Å^3)	−21 ± 2	−17 ± 2
	−3 ± 2	−9 ± 2
ΔH (eV)	−0.8 ± 0.1	−0.70 ± 0.08
	+0.4 ± 0.3	+0.3 ± 0.3
$-T\Delta S$ (eV)	+0.17 ± 0.1	0 ± 0.1
	−0.54 + 0.3	−0.37 ± 0.3

[a] The thermodynamic parameters in each row in the column are from the ref *35* for producing the $P_{700}{}^+A_1{}^-$ from $P_{700}{}^*$ and the $P_{700}{}^+F_{A/B}{}^-$ from $P_{700}{}^+A_1{}^-$ in the wild-type PS I, respectively. [b] The values in the column represent the thermodynamic parameters for the formation of $P_{700}{}^*$ to $P_{700}{}^+A_P{}^-$ and of the $P_{700}{}^+A_P{}^-$ to $P_{700}{}^+F_{A/B}{}^-$ in the *menA*/*B* PS I, respectively, where the volume change, enthalpy, and entropy of the latter step are inferred assuming the overall reaction of the production of $P_{700}{}^+F_{A/B}{}^-$ from $P_{700}{}^*$ is the same as that of the wild type.

The smaller volume contraction may be caused by the following two factors: compressibility of protein and polarity of quinone pocket. The first factor is the effect of the foreign plastoquinone on the compressibility of the local environment of the protein. The orientation and distance of plastoquinone-9 in the mutants are known to be similar to phylloquinone in the wild-type PS I (*20*). However, since the pocket of A_1 is adapted to phylloquinone, the smaller plastoquinone with the longer tail may not fit well into the protein. If the effect of the larger tail is to crowd the hydrophobic site, this could decrease the compressibility of the local domain and so decrease ΔV_{el}. Alternatively, the A_1 binding region in *menA*/*B* PS I may be more polar; i.e., it has a larger effective ε, compared to the wild-type PS I. This could be due to the small size of plastoquinone-9, allowing a water molecule to be present. This possibility also could explain the change in potential of the quinone because of hydrogen bonding to the water.

Free Energy, Enthalpy, and Entropy. The driving force of electron transfer (ΔG) can be directly determined from the difference of the *in situ* redox potentials of the cofactors (measured separately, however). The trap energy of PS I is estimated as the energy of exciting light, 1.77 eV, and from the redox potential of P_{700} reported in the literature, +0.45 V (*35, 54*). However, knowledge of the redox potential of plastoquinone-9 in the *menA* and *menB* mutants is required to calculate the free energy of electron transfer associated with A_P. There are no directly measured data available. By use of the electron transfer theory and kinetic data, the redox potential of plastoquinone at the A_1 site was estimated to be −0.61 V (*21, 55*). However, we believe the error to be at least 0.1 V. The ΔG for producing $P_{700}{}^+A_P{}^-$ from $P_{700}{}^*$ is then −0.71 eV. Similarly, the free energy for producing $P_{700}{}^+F_{A/B}{}^-$ from $P_{700}{}^*F_{A/B}$ is −0.77 eV (*35*). Thus we infer that the free energy of $P_{700}{}^+A_P{}^-F_{A/B}$ to $P_{700}{}^+A_PF_{A/B}{}^-$ reaction is −0.06 ± 0.10 eV in the mutants (Table 3).

Pulsed photoacoustics provides directly the enthalpy change of electron transfer reactions in PS I. Knowing the free energy of the electron transfer step in wild-type PS I and *menA*/*B* PS I, the entropic contribution ($T\Delta S$) can be determined by the Gibbs relation $\Delta G = \Delta H - T\Delta S$. As shown in Tables 1 and 2, the enthalpy change occurring on

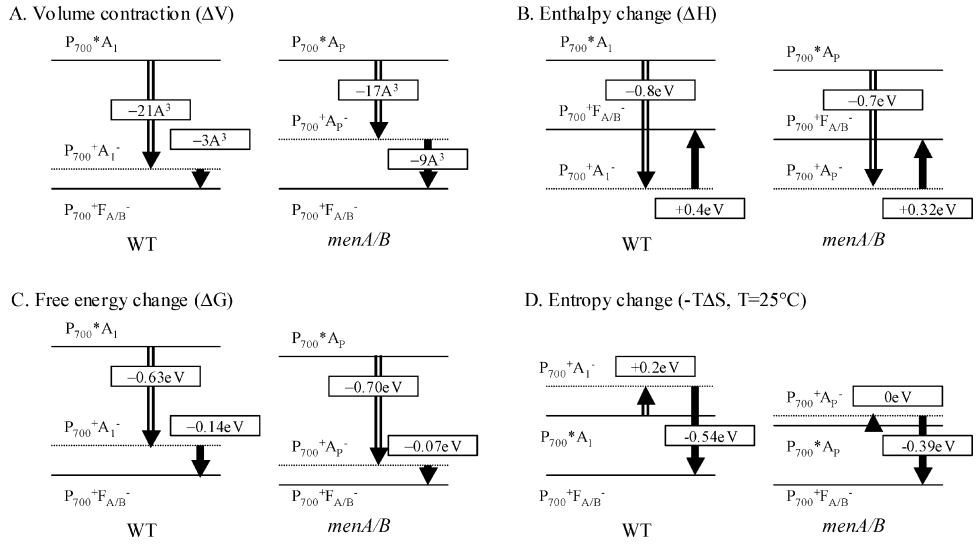

FIGURE 7: Thermodynamic parameters of charge separation in *menA/B* PS I and wild-type PS I from *Synechocystis* 6803. Panel A shows the volume contractions of charge separation. Panel B shows enthalpy changes of photoreaction in PS I measured by either nanosecond or microsecond photoacoustics. Panel C shows free energy changes based on the redox potentials of each individual cofactor in situ. Panel D shows the apparent entropy changes calculated by the thermodynamic relation $\Delta G = \Delta H - T\Delta S$. The solid lines (—) represent the excited state of P_{700} and final state of $P_{700}{}^{+}F_{A/B}{}^{-}$, respectively. The dash lines (•••) are the intermediate state of $P_{700}{}^{+}A_1{}^{-}$ (WT) or $P_{700}{}^{+}A_P{}^{-}$ (mutants). The open arrows (⟹) are the reaction forming $P_{700}{}^{+}A_1{}^{-}$ (WT) or $P_{700}{}^{+}A_p{}^{-}$ (mutants) from P_{700}* and the closed arrows (→) the following reaction producing $P_{700}{}^{+}F_{A/B}{}^{-}$ from P_{700}*.

the formation of $P_{700}{}^{+}A_P{}^{-}$ from P_{700}* in *menA/B* PS I is −0.7 ± 0.07 eV. This is close to the estimated free energy of this reaction (−0.70 eV), and thus the apparent entropy change is close to zero (Table 3). Considering the enthalpy change (−0.4 eV) of the overall reaction for the formation of $P_{700}{}^{+}F_{A/B}{}^{-}$ from P_{700}* in the wild-type PS I, we infer that the electron transfer reaction from $A_P{}^{-}$ to $F_{A/B}$ would be associated with a positive enthalpy change of +0.3 eV and thus is completely entropy driven as the free energy is zero in the mutants. The environmental changes postulated to explain the volume changes could affect the enthalpy changes.

The entropy of electron transfer reactions is often assumed to be zero. However, the free energy calculated from kinetic measurements of reverse electron transfer in bacterial reaction centers shows that the free energy is time- and temperature-dependent, particularly on the less than nanosecond time scale (*56*−*58*). The kinetics of these decays can only be described as "distributed", and simple analysis in terms of a single component is not trustworthy. Protein dynamics may play a key role in this electron transfer step (*59*). However, the question of whether these "relaxations" are enthalpy and/or entropy driven remains to be answered. The slow (microsecond) component observed in wild-type PS I could be such a relaxation, but only the ΔV was determined. We have labeled the difference between observed enthalpies and estimated free energies as entropies to highlight the problem. In addition to reaction centers of *Rb. sphaeroides* (*18*), we have observed similar positive entropic contribution in PS I preparations of *Synechocystis* sp. PCC 6803 (*32*), but not in PS II preparations (*33*). Charge movement, but not charge separation due to proton transfer, may be the difference in PS II on the 1 μs time scale. Clear-cut and large negative entropic contribution is seen in the model system of triplet porphyrin-to-ferricyanide electron transfer in aqueous solution (*31*), where "relaxations" are too fast to be relevant.

To summarize the thermodynamic data, we present the volume changes, free energies, and enthalpy and entropy changes on *menA/B* PS I in comparison with those on the wild-type PS I in Figure 7. Opened arrows are the early step forming $P_{700}{}^{+}A_1{}^{-}$ from P_{700}* for the wild-type PS I or $P_{700}{}^{+}A_P{}^{-}$ from P_{700}* for the mutants, and solid arrows are the number of the following reaction: $P_{700}{}^{+}A_P{}^{-} \rightarrow P_{700}{}^{+}F_{A/B}{}^{-}$. As shown in panel A, the volume contraction of the early step of the photoreaction in the mutants (−17 Å^3) is smaller than that in the wild type (−21 Å^3). Similarly, the enthalpy change (−0.7 eV) of the early step in the mutants is smaller than that (−0.8 eV) in wild-type PS I (Figure 7B). Assuming a redox potential of −0.6 V for plastoquinone-9 in the A_1 site (*21*), the free energy (−0.7 eV) of this early reaction in the mutants is larger than the value (−0.6 eV) in the wild type as indicated in Figure 7C. Taking the difference of free energy and enthalpy change in the mutants, the apparent entropy change of the early step in mutants is zero. In contrast, the apparent entropy change in the wild type is calculated to be +0.2 eV. Since the apparent entropy change for the overall reaction of the generation of $P_{700}{}^{+}F_{A/B}{}^{-}$ from P_{700}* is +0.35 eV (*32*), it implies that the latter reaction in the mutants, i.e., the $P_{700}{}^{+}A_P{}^{-}F_{A/B} \rightarrow P_{700}{}^{+}A_PF_{A/B}{}^{-}$ reaction, is almost completely entropy driven ($T\Delta S = +0.4$ eV and $\Delta G = -0.1$ eV) (Figure 7D). Therefore, on the basis of our experimental results we propose that the foreign quinone (A_P) in PS I does affect the thermodynamics of charge separation in the early steps in PS I with a smaller volume and enthalpy changes, a large free energy, and zero entropy change.

The driving force of electron transfer in photosynthetic systems is not only dependent on the bonding energy of the cofactor and interaction energy with the protein (enthalpy) but also dependent on the available states of interaction with the protein (entropy). Entropy changes are important to completely understand the molecular mechanisms of electron and/or proton transfer in condensed phases, in particular when proteins are involved, and photoacoustics is a direct way to ferret them out.

ACKNOWLEDGMENT

We thank Irene Zielinski-Large for technical assistance.

REFERENCES

1. Ort, D. R., and Yocum, C. F. (1996) *Oxygenic Photosynthesis: The Light Reactions*, Springer, Dordrecht.
2. Kamlowski, A., Altenberg-Greulich, B., Van der Est, A., Zech, S. G., Bittl, R., Fromme, P., Lubitz, W., and Stehlik, D. (1998) The quinone acceptor A_1 in photosystem I: Binding site, and comparison to Q_A in purple bacteria reaction centers. *J. Phys. Chem. B 102*, 8278–8287.
3. van der Est, A., Sieckmann, I., Lubitz, W., and Stehlik, D. (1995) Differences in the binding of the primary quinone acceptor in photosystem I and reaction centers of *Rhodobacter sphaeroides*-R26 studied with transient EPR spectroscopy. *Chem. Phys. 194*, 349–359.
4. Golbeck, J. H. (2006) *Photosystem I: The Light-Driven Plastocyanin:Ferredoxin Oxioreductase*, Springer, Dordrecht.
5. Chitnis, P. R. (2001) Photosystem I: function and physiology. *Annu. Rev. Plant Physiol. Plant Mol. Biol. 52*, 593–626.
6. Gobets, B., and van Grondelle, R. (2001) Energy transfer and trapping in photosystem I. *Biochim. Biophys. Acta 1507*, 80–99.
7. Brettel, K., and Leibl, W. (2001) Electron transfer in photosystem I. *Biochim. Biophys. Acta 1507*, 100–114.
8. Jordan, P., Fromme, P., Witt, H. T., Klukas, O., Saenger, W., and Krauss, N. (2001) Three-dimensional structure of cyanobacterial photosystem I at 2.5 Å resolution. *Nature 411*, 909–917.
9. Amunts, A., Drory, O., and Nelson, N. (2007) The structure of a plant photosystem I supercomplex at 3.4 Å resolution. *Nature 447*, 58–63.
10. Joliot, P., and Joliot, A. (1999) In vivo analysis of the electron transfer within photosystem I: are the two phylloquinones involved? *Biochemistry 38*, 11130–11136.
11. Guergova-Kuras, M., Boudreaux, B., Joliot, A., Joliot, P., and Redding, K. (2001) Evidence for two active branches for electron transfer in photosystem I. *Proc. Natl. Acad. Sci. U.S.A. 98*, 4437–4442.
12. Bautista, J. A., Rappaport, F., Guergova-Kuras, M., Cohen, R. O., Golbeck, J. H., Wang, J. Y., Beal, D., and Diner, B. A. (2005) Biochemical and biophysical characterization of photosystem I from phytoene desaturase and ζ-carotene desaturase deletion mutants of *Synechocystis* sp. PCC 6803: evidence for PsaA- and PsaB-side electron transport in cyanobacteria. *J. Biol. Chem. 280*, 20030–20041.
13. Cohen, R. O., Shen, G., Golbeck, J. H., Xu, W., Chitnis, P. R., Valieva, A. I., van der Est, A., Pushkar, Y., and Stehlik, D. (2004) Evidence for asymmetric electron transfer in cyanobacterial photosystem I: analysis of a methionine-to-leucine mutation of the ligand to the primary electron acceptor A_0. *Biochemistry 43*, 4741–4754.
14. Xu, W., Chitnis, P. R., Valieva, A., van der Est, A., Brettel, K., Guergova-Kuras, M., Pushkar, Y. N., Zech, S. G., Stehlik, D., Shen, G., Zybailov, B., and Golbeck, J. H. (2003) Electron transfer in cyanobacterial photosystem I: II. Determination of forward electron transfer rates of site-directed mutants in a putative electron transfer pathway from A_0 through A_1 to F_X. *J. Biol. Chem. 278*, 27876–27887.
15. Xu, W., Chitnis, P., Valieva, A., van der Est, A., Pushkar, Y. N., Krzystyniak, M., Teutloff, C., Zech, S. G., Bittl, R., Stehlik, D., Zybailov, B., Shen, G., and Golbeck, J. H. (2003) Electron transfer in cyanobacterial photosystem I: I. Physiological and spectroscopic characterization of site-directed mutants in a putative electron transfer pathway from A_0 through A_1 to F_X. *J. Biol. Chem. 278*, 27864–27875.
16. Dashdorj, N., Xu, W., Cohen, R. O., Golbeck, J. H., and Savikhin, S. (2005) Asymmetric electron transfer in cyanobacterial photosystem I: charge separation and secondary electron transfer dynamics of mutations near the primary electron acceptor A_0. *Biophys. J. 88*, 1238–1249.
17. Gunner, M. R., and Dutton, P. L. (1989) Temperature and $-\Delta G$ dependence of the electron transfer from BPh^- to Q_A in reaction center protein from *Rhodobacter sphaeroides* with different quinones as Q_A. *J. Am. Chem. Soc. 111*, 3400–3412.
18. Edens, G. J., Gunner, M. R., Xu, Q., and Mauzerall, D. (2000) The enthalpy and entropy of reaction for formation of $P^+Q_A^-$ from excited reaction centers of *Rhodobacter sphaeroides*. *J. Am. Chem. Soc. 122*, 1479–1485.
19. Johnson, T. W., Shen, G., Zybailov, B., Kolling, D., Reategui, R., Beauparlant, S., Vassiliev, I. R., Bryant, D. A., Jones, A. D., Golbeck, J. H., and Chitnis, P. R. (2000) Recruitment of a foreign quinone into the A_1 site of photosystem I. I. Genetic and physiological characterization of phylloquinone biosynthetic pathway mutants in *Synechocystis* sp. PCC 6803. *J. Biol. Chem. 275*, 8523–8530.
20. Zybailov, B., van der Est, A., Zech, S. G., Teutloff, C., Johnson, T. W., Shen, G., Bittl, R., Stehlik, D., Chitnis, P. R., and Golbeck, J. H. (2000) Recruitment of a foreign quinone into the A_1 site of photosystem I. II. Structural and functional characterization of phylloquinone biosynthetic pathway mutants by electron paramagnetic resonance and electron-nuclear double resonance spectroscopy. *J. Biol. Chem. 275*, 8531–8539.
21. Semenov, A. Y., Vassiliev, I. R., van Der Est, A., Mamedov, M. D., Zybailov, B., Shen, G., Stehlik, D., Diner, B. A., Chitnis, P. R., and Golbeck, J. H. (2000) Recruitment of a foreign quinone into the A_1 site of photosystem I. Altered kinetics of electron transfer in phylloquinone biosynthetic pathway mutants studied by time-resolved optical, EPR, and electrometric techniques. *J. Biol. Chem. 275*, 23429–23438.
22. Mauzerall, D., Hou, J. M., and Boichenko, V. A. (2002) Volume changes and electrostriction in the primary photoreactions of various photosynthetic systems: estimation of dielectric coefficient in bacterial reaction centers and of the observed volume changes with the Drude-Nernst equation. *Photosynth. Res. 74*, 173–180.
23. Delosme, R. (2003) On some aspects of photosynthesis revealed by photoacoustic studies: a critical evaluation. *Photosynth. Res. 76*, 289–301.
24. Braslavsky, S. E., and Heibel, G. E. (1992) Time-resolved photothermal and photoacoustic methods applied to photoinduced processes in solution. *Chem. Rev. 92*, 1381–1410.
25. Strassburger, J. M., Gartner, W., and Braslavsky, S. E. (1997) Volume and enthalpy changes after photoexcitation of bovine rhodopsin: laser-induced optoacoustic studies. *Biophys. J. 72*, 2294–2303.
26. Borsarelli, C. D., and Braslavsky, S. E. (1998) Volume changes correlate with enthalpy changes during the photoinduced formation of the 3MLCT state of ruthenium(II) bipyridine cyano complexes in the presence of salts: A case of the entropy-enthalpy compensation effect. *J. Phys. Chem. B 102*, 6231–6238.
27. Rizzi, A. C., van Gastel, M., Liddell, P. A., Palacios, R. E., Moore, G. F., Kodis, G., Moore, A. L., Moore, T. A., Gust, D., and Braslavsky, S. E. (2008) Entropic changes control the charge separation process in triads mimicking photosynthetic charge separation. *J. Phys. Chem. A 112*, 4215–4223.
28. Losi, A., Yruela, I., Reus, M., Holzwarth, A. R., and Braslavsky, S. E. (2003) Structural changes upon excitation of D1-D2-Cyt b_{559} photosystem II reaction centers depend on the beta-carotene content. *Photochem. Photobiol. Sci. 2*, 722–729.
29. Losi, A., Wegener, A. A., Engelhard, M., and Braslavsky, S. E. (2001) Enthalpy-entropy compensation in a photocycle: The K-to-L transition in sensory rhodopsin II from *Natronobacterium pharaonis*. *J. Am. Chem. Soc. 123*, 1766–1767.
30. Mauzerall, D., Feitelson, J., and Prince, R. (1995) Wide band, time-resolved photoacoustic study of electron transfer reactions: difference between measured enthalpies and redox free energies. *J. Phys. Chem. 99*, 1090–1093.
31. Feitelson, J., and Mauzerall, D. (2002) Enthalpy and electrostriction in the electron transfer reaction between triplet zinc uroporphyrin and ferricyanide. *J. Phys. Chem. B 106*, 9674–9678.
32. Hou, J. M., Boichenko, V. A., Wang, Y. C., Chitnis, P. R., and Mauzerall, D. (2001) Thermodynamics of electron transfer in oxygenic photosynthetic reaction centers: a pulsed photoacoustic study of electron transfer in photosystem I reveals a similarity to bacterial reaction centers in both volume change and entropy. *Biochemistry 40*, 7109–7116.
33. Hou, J. M., Boichenko, V. A., Diner, B. A., and Mauzerall, D. (2001) Thermodynamics of electron transfer in oxygenic photosynthetic reaction centers: volume change, enthalpy, and entropy of electron-transfer reactions in manganese-depleted photosystem II core complexes. *Biochemistry 40*, 7117–7125.
34. Boichenko, V. A., Hou, J. M., and Mauzerall, D. (2001) Thermodynamics of electron transfer in oxygenic photosynthetic reaction centers: volume change, enthalpy, and entropy of electron-transfer reactions in the intact cells of the cyanobacterium *Synechocystis* PCC 6803. *Biochemistry 40*, 7126–7132.

35. Hou, H. J. M., and Mauzerall, D. (2006) The A^-F_X to $F_{A/B}$ step in *Synechocystis* 6803 photosystem I is entropy driven. *J. Am. Chem. Soc. 128*, 1580–1586.
36. Mauzerall, D. (2006) Thermodynamics in photosystem I, in *Photosystem I: The Light-Driven Plastocyanin:Ferredoxin Oxidoreductase* (Golbeck, J., Ed.) pp 571−581, Springer, Dordrecht.
37. Herbert, S. K., Han, T., and Vogelmann, T. C. (2001) New applications of photoacoustics to the study of photosynthesis. *Photosynth. Res. 66*, 13–31.
38. Malkin, S. (1996) The photoacoustic method in photosynthesis—monitoring and analysis of phenomena which lead to pressure changes following light excitation. *Adv. Photosynth. 3*, 191–206.
39. Nagy, L., Kiss, V., Brumfeld, V., and Malkin, S. (2001) Thermal and structural changes of photosynthetic reaction centers characterized by photoacoustic detection with a broad frequency band hydrophone. *Photochem. Photobiol. 74*, 81–87.
40. Zhang, D., and Mauzerall, D. (1996) Volume and enthalpy changes in the early steps of bacteriorhodopsin photocycle studied by time-resolved photoacoustics. *Biophys. J. 71*, 381–388.
41. Mauzerall, D., Hou, J.-M., and Boichenko, V. A. (2002) Volume changes and electrostriction in the primary photoreactions of various photosynthetic systems: estimation of dielectric coefficient in bacterial reaction centers and of the observed volume changes with the Drude-Nernst equation. *Photosynth. Res. 74*, 173–180.
42. Delosme, R., Beal, D., and Joliot, P. (1994) Photoacoustic detection of flash-induced charge separation in photosynthetic systems. Spectral dependence of the quantum yield. *Biochim. Biophys. Acta 1185*, 56–64.
43. Santabarbara, S., Heathcote, P., and Evans, M. C. (2005) Modelling of the electron transfer reactions in photosystem I by electron tunnelling theory: the phylloquinones bound to the PsaA and the PsaB reaction center subunits of PS I are almost isoenergetic to the iron-sulfur cluster F_X. *Biochim. Biophys. Acta 1708*, 283–310.
44. Sun, J., Ke, A., Jin, P., Chitnis, V. P., and Chitnis, P. R. (1998) Isolation and functional study of photosystem I subunits in the cyanobacterium *Synechocystis* sp. PCC 6803. *Methods Enzymol. 297*, 124–139.
45. Rudzki, S. J., Libertini, L. J., and Small, E. W. (1992) Analysis of photoacoustic waveforms using fluorescent decay analysis techniques. *Biophys. Chem. 42*, 29–48.
46. Setif, P., and Brettel, K. (1993) Forward electron transfer from phylloquinone A_1 to iron-sulfur centers in spinach photosystem I. *Biochemistry 32*, 7846–7854.
47. Schlodder, E., Falkenberg, K., Gergeleit, M., and Brettel, K. (1998) Temperature dependence of forward and reverse electron transfer from A_1^-, the reduced secondary electron acceptor in photosystem I. *Biochemistry 37*, 9466–9476.
48. Brettel, K., and Vos, M. H. (1999) Spectroscopic resolution of the picosecond reduction kinetics of the secondary electron acceptor A_1 in photosystem I. *FEBS Lett. 447*, 315–317.
49. Golbeck, J. H. (1999) A comparative analysis of the spin state distribution of *in vitro* and *in vivo* mutants of PsaC: A biochemical argument for the sequence of electron transfer in photosystem I as $F_X \rightarrow F_A \rightarrow F_B \rightarrow$ ferredoxin/flavodoxin. *Photosynth. Res. 61*, 107–144.
50. Vassiliev, I. R., Antonkine, M. L., and Golbeck, J. H. (2001) Iron-sulfur clusters in type I reaction centers. *Biochim. Biophys. Acta 1507*, 139–160.
51. Drude, P., and Nernst, W. (1894) Über elektrostriktion durch freie ionen. *Z. Phys. Chem. 15*, 79–85.
52. Johnson, T. W., Zybailov, B., Jones, A. D., Bittl, R., Zech, S., Stehlik, D., Golbeck, J. H., and Chitnis, P. R. (2001) Recruitment of a foreign quinone into the A_1 site of photosystem I. In vivo replacement of plastoquinone-9 by media-supplemented naphthoquinones in phylloquinone biosynthetic pathway mutants of *Synechocystis* sp. PCC6803. *J. Biol. Chem. 276*, 39512–39521.
53. Johnson, T. W., and Golbeck, J. H. (2004) Biological incorporation of alternative quinones into photosystem I, in *CRC Handbook of Organic Photochemistry and Photobiology*, 2nd ed., pp 119/111−119/114, CRC Press, Boca Raton, FL.
54. Brettel, K. (1997) Electron transfer and arrangement of the redox cofactors in photosystem I. *Biochim. Biophys. Acta 1318*, 322–373.
55. Karyagina, I., Pushkar, Y., Stehlik, D., van der Est, A., Ishikita, H., Knapp, E.-W., Jagannathan, B., Agalarov, R., and Golbeck, J. H. (2007) Contributions of the protein environment to the midpoint potentials of the A_1 phylloquinones and the F_X iron-sulfur cluster in photosystem I. *Biochemistry 46*, 10804–10816.
56. Peloquin, J. M., Williams, J. C., Lin, X., Alden, R. G., Taguchi, A. K. W., Allen, J. P., and Woodbury, N. W. (1994) Time-dependent thermodynamics during early electron transfer in reaction centers from *Rhodobacter sphaeroides*. *Biochemistry 33*, 8089–8100.
57. Woodbury, N. W., Peloquin, J. M., Alden, R. G., Lin, X., Lin, S., Taguchi, A. K. W., Williams, J. C., and Allen, J. P. (1994) Relationship between thermodynamics and mechanism during photoinduced charge separation in reaction centers from *Rhodobacter sphaeroides*. *Biochemistry 33*, 8101–8112.
58. Xu, Q., and Gunner, M. R. (2000) Temperature dependence of the free energy, enthalpy, and entropy of $P^+Q_A^-$ charge recombination in *Rhodobacter sphaeroides* R-26 reaction centers. *J. Phys. Chem. B 104*, 8035–8043.
59. Wang, H., Lin, S., Allen, J. P., Williams, J. C., Blankert, S., Laser, C., and Woodbury, N. W. (2007) Protein dynamics control the kinetics of initial electron transfer in photosynthesis. *Science 316*, 747–750.
60. Liu, Y., Edens, G. J., Grzymski, J., and Mauzerall, D. (2008) Volume and enthalpy changes of proton transfers in the bacteriorhodopsin photocycle studied by millisecond time-resolved photopressure measurements. *Biochemistry 47*, 7752–7761.

BI801951T